Annals of Botany **122**: 777–789, 2018
doi: 10.1093/aob/mcx178, available online at www.academic.oup.com/aob

ANNALS OF BOTANY
Founded 1887

PART OF A SPECIAL ISSUE ON FUNCTIONAL–DEVELOPMENTAL PLANT CELL BIOLOGY

Arabidopsis thaliana plants lacking the ARP2/3 complex show defects in cell wall assembly and auxin distribution

Vaidurya Pratap Sahi[1]†‡, Petra Cifrová[1]†, Judith García-González[1], Innu Kotannal Baby[2], Gregory Mouillé[3], Emilie Gineau[3], Karel Müller[2], František Baluška[4], Aleš Soukup[1], Jan Petrášek[1,2] and Kateřina Schwarzerová[1]*

[1]Department of Experimental Plant Biology, Faculty of Science, Charles University, Viničná 5, Czech Republic, [2]Institute of Experimental Botany, AS CR, Rozvojová 263, Czech Republic, [3]Institut Jean-Pierre Bourgin, INRA, AgroParisTech, CNRS, Université Paris-Saclay, 78000 Versailles, France and [4]Department of Plant Cell Biology, Institute of Cellular and Molecular Botany, University of Bonn, Kirschallee 1, Bonn, Germany
†These authors contributed equally to this work.
‡Current address: Karlsruhe Institute of Technology, Botanical Institute, Fritz-Haber-Weg 4, Karlsruhe, Germany
**For correspondence. E-mail schwarze@natur.cuni.cz*

Received: 30 August 2017 Returned for revision: 2 October 2017 Editorial decision: 24 October 2017 Accepted: 10 November 2017
Published electronically 25 December 2017

• **Background and Aim** The cytoskeleton plays an important role in the synthesis of plant cell walls. Both microtubules and actin cytoskeleton are known to be involved in the morphogenesis of plant cells through their role in cell wall building. The role of ARP2/3-nucleated actin cytoskeleton in the morphogenesis of cotyledon pavement cells has been described before. Seedlings of *Arabidopsis* mutants lacking a functional ARP2/3 complex display specific cell wall-associated defects.
• **Methods** In three independent *Arabidopsis* mutant lines lacking subunits of the ARP2/3 complex, phenotypes associated with the loss of the complex were analysed throughout plant development. Organ size and anatomy, cell wall composition, and auxin distribution were investigated.
• **Key Results** ARP2/3-related phenotype is associated with changes in cell wall composition, and the phenotype is manifested especially in mature tissues. Cell walls of mature plants contain less cellulose and a higher amount of homogalacturonan, and display changes in cell wall lignification. Vascular bundles of mutant inflorescence stems show a changed pattern of AUX1-YFP expression. Plants lacking a functional ARP2/3 complex have decreased basipetal auxin transport.
• **Conclusions** The results suggest that the ARP2/3 complex has a morphogenetic function related to cell wall synthesis and auxin transport.

Keywords: ARP2/3, *Arabidopsis thaliana*, cell wall, cellulose, pectin, lignin, morphogenesis, auxin, AUX1

INTRODUCTION

Plant cell shape is primarily dependent on the cell wall. The plant cell wall is a rigid structure on which the plant protoplast exerts turgor pressure (Cosgrove, 2005). Although turgor pressure remains constant during plant cell growth, the cell wall is locally modified and assembled to produce regions with higher or lower plasticity (Cosgrove, 2005; Szymanski and Cosgrove, 2009). This is believed to be the key mechanism leading to the growth and morphogenesis of individual plant cells. Therefore, understanding the mechanisms controlling plant cell wall assembly and dynamics is pivotal to understanding plant morphogenesis.

The cytoskeleton is a dynamic protein structure involved in transport of organelles and processes of cell shaping in all eukaryotic cells. In plants, the cytoskeleton is known to control cell wall assembly. It has been well established that microtubules play a major role in the deposition of cellulose microfibrils into the cell wall; early observations noted parallel orientation of cortical microtubules and cellulose microfibrils in plant cells (Ledbetter and Porter, 1963). More recent observations confirmed the role of microtubules in guiding movement of the cellulose synthase (CESA) enzyme complex in the plasma membrane, controlling the orientation of newly deposited cellulose (Paredez *et al.*, 2006; Li *et al.*, 2012). The role of the actin cytoskeleton in the growth and polarity of tip-growing cells has been widely investigated. It is clear that the actin cytoskeleton is one of the main determinants needed for the growth and polarity of tip-growing cells such as pollen tubes and root hairs (Baluška *et al.*, 2000; Ketelaar, 2013; Vazquez *et al.*, 2014; Hepler and Winship, 2015). Actin filaments are involved in the transport of exocytic vesicles delivering the cell wall material from Golgi apparatus to the cell wall in tip-growing cells (Kim and Brandizzi, 2014; Rounds *et al.*, 2014; Gendre *et al.*, 2015). The actin cytoskeleton also participates in the anisotropic growth of a plant cell. However, the mechanism of its function in building the cell wall is only partially understood. Similar

to polar growth, actin filaments are necessary for delivery of vesicles containing cell wall components to the plasma membrane and the cell wall. This was supported by studies in which plant growth was severely inhibited either by interfering with actin polymerization (Baluska *et al.*, 2001) or by knocking out several myosin genes (Peremyslov *et al.*, 2010). A general actomyosin-driven cytoplasmic streaming was shown to contribute to plant cell expansion, confirming the importance of the actin cytoskeleton in the distribution and delivery of cell wall material to growing cell walls (Peremyslov *et al.*, 2015). The role of individual actin isotypes was demonstrated by Kandasamy *et al.* (2009), where multiple defects in cellular and organ morphology and root hair development were observed. Moreover, 5-d-old etiolated seedlings of *act2act7* mutants contained less cellulose and displayed altered delivery of post-Golgi apparatus CESA containing vesicles to the plasma membrane (PM) and modified the lifetime of CESA complexes in the PM, suggesting involvement of the actin cytoskeleton in cellulose synthesis (Sampathkumar *et al.*, 2013).

Seedlings of *Arabidopsis* mutants lacking a functional ARP2/3 complex display phenotypes suggesting a role of ARP2/3-controlled actin nucleation in cell wall synthesis. Defects in the cotyledon pavement cell shape and cotyledon and hypocotyl cell–cell adhesion were reported for mutants lacking ARP2/3 complex subunits (Le *et al.*, 2003; Mathur *et al.*, 2003*a, b*; El-Assal *et al.*, 2004*a*; Kotchoni *et al.*, 2009; Zhang *et al.*, 2013*b*) as well as in mutants lacking subunits of ARP2/3-activating complex WAVE/SCAR (Qiu *et al.*, 2002; El Assal *et al.*, 2004*b*; Basu *et al.*, 2005, 2008; Zhang *et al.*, 2005; Djakovic *et al.*, 2006). A typical phenotype of all these mutants is characterized by distorted trichomes (Mathur *et al.*, 1999; Szymanski *et al.*, 1999; Le *et al.*, 2003; Li *et al.*, 2003; Schwab *et al.*, 2003; Basu *et al.*, 2004, 2005; El-Assal *et al.*, 2004*a*, *b*). This phenotype has been associated with cytoskeleton organization-based defective deposition of the cell wall in growing trichomes (Yanagisawa *et al.*, 2015). In root tips of *brk1* (Djakovic *et al.*, 2006; Le *et al.*, 2006) and *arp2* (Li *et al.*, 2003) mutants, occasional changes in cell wall deposition were reported; for example, abnormal deposition of the cell wall material was observed in three-way junctions between cells (Dyachok *et al.*, 2008). However, no changes in the carbohydrate composition of the cell wall were found in seedlings of several distorted mutants such as *brk1* and *arp2* (Dyachok *et al.*, 2008) or *spk1-1* (Qiu *et al.*, 2002).

The morphogenesis of walled plant cells with complex shapes requires the proper coordination of executive structures such as the cytoskeleton with signalling pathways determining the polarity of cell expansion. This coordination depends on the plant hormone auxin's directional cell-to-cell transport, which defines numerous morphogenic effects, including polarity establishment (Shao and Dong, 2016). Recent progress in our understanding of mutual interactions between actin and auxin revealed several developmental regulatory loops that include both transcriptional and post-transcriptional processes (Nick, 2009; Durst *et al.*, 2013; Zhu and Geisler, 2015; Eggenberger *et al.*, 2017). Through its effect on the localization of auxin carriers, actin plays an important integration role for other phytohormonal pathways, as shown for the auxin efflux carrier PIN2 and brassinosteroids (Lanza *et al.*, 2012). The extensibility of the cell wall increases upon auxin-induced extrusion of protons into the apoplast, which is associated with the action of PM H^+ATPases and acidification of the apoplast (Hager *et al.*, 1991; Takahashi *et al.*, 2012; Barbez *et al.*, 2017). Both these processes have been recently shown to be triggered by TIR1-mediated auxin signalling in *Arabidopsis* hypocotyls (Fendrych *et al.*, 2016). Moreover, auxin locally modifies mechanical properties of the cell wall, thus enabling morphogenesis of walled cells (Braybrook and Peaucelle, 2013). Disruption of auxin transport is accompanied by low differentiation of plant tissues and formation of thinner cell walls (Ranocha *et al.*, 2010, 2013). On the other hand, mechanical properties of the cell wall may modulate auxin signalling by affecting the localization of auxin efflux carrier PIN1 (Feraru *et al.*, 2011; Nakayama *et al.*, 2012; Braybrook and Peaucelle, 2013).

Most studies of ARP2/3 complex mutants have focused on changes in the early stages of development of plant seedlings. Here, we compared phenotypes of three independent mutants, *arp2*, *arpc4* and *arpc5*, in several developmental stages. Well-known defects in trichome shape and cell–cell adhesion were clearly detectable in all tested mutant plants in both cotyledons and true leaves. On the other hand, increased circularity of cotyledon epidermal pavement cells was not observed in true leaves. The mutants showed a decreased thickness of mature organs, i.e. leaves and inflorescence stems. The cell wall in inflorescence stems was thinner in mutants and changes in the deposition of lignin were observed as well. Biochemical analysis revealed a decreased amount of cellulose and increased homogalacturonan fraction in inflorescence stem cell walls, while no changes were detected in young seedlings. Changes to inflorescence stem cell walls were accompanied by reduced basipetal auxin transport in the inflorescence stems and decreased amount of auxin influx carrier AUX1 in the provasculature. Our analysis shows that the ARP2/3 complex plays a role in the control of cell wall synthesis and auxin-controlled morphogenesis in plants.

MATERIALS AND METHODS

Plant material

Arabidopsis thaliana plants were grown in peat pellets under a photoperiod of 16: 8 h and 23 °C. For *in vitro* cultivation, plants were grown on vertical agar plates with half-strength Murashige and Skoog medium (MS/2) supplemented with 1 % (w/v) sucrose. *Arabidopsis thaliana* lines used in this study were Col-0 (WT), SALK_077920.56.00 (*arp2*), SALK_013909.27.65 (*arpc4*) and SALK_123936.41.55 (*arpc5*), obtained from NASC T-DNA mutant collection (Scholl *et al.*, 2000). Plants carrying *DR5::GUS* (Ulmasov *et al.*, 1997) or *AUX1::AUX1:YFP* (Swarup *et al.*, 2004) were crossed with the *arpc5* mutant line, and homozygous *arpc5* plants expressing the reporter gene selected from an F_2 generation were used. All mutants were genotyped for homozygosity; primers used and details of PCR and qRT-PCR are shown in Supplementary Data Fig. S1.

Resin-embedded sectioning of cotyledons

Fourteen-day-old cotyledons were fixed [50 mM Na-cacodylate buffer (NCB), 2 % glutaraldehyde, 1 %

paraformaldehyde, 1 % DMSO, 0.1 M sucrose] for 45–60 min under low pressure. Samples were then washed in 100 mM NCB three times for 15 min and post-fixed in 1 % OsO_4 for 45 min. Samples were gradually dehydrated in an acetone series. Samples were further infiltrated in a solution of acetone/vinyl cyclohexene dioxide (ERL), 3: 1, overnight. This was followed by the incubation in acetone/ERL 1: 1 for 4 h, acetone/ERL 1: 3 for 4 h and finally the samples were kept overnight in pure ERL. The resin was heat hardened at 70 °C and samples were sectioned using an ultramicrotome to 2 µm. Sections on glass slides were stained in a methylene blue – azure II staining solution [1 % methylene blue and 1 % borax in distilled water mixed with 1 % azure II in distilled water 1: 1 (v/v)] for a few seconds on a hot plate (50–55 °C). Samples were washed with distilled water and observed using an Olympus Provis AX 70 transmitted light microscope.

Hand sectioning

Transverse sections 200 µm thick were taken from the base of 6-week-old inflorescence stems and the midrib region in the central part of freshly harvested 5th mature leaves using a hand microtome. The sections were immediately stained in 0.01 % aqueous solution of calcofluor white (CW) or 0.5 % aqueous solution of toluidine blue O (TBO) solutions for 2 min (Soukup, 2014). Lignin detection was performed in 1 % (w/v) phloroglucinol in 18 % HCl until sections were stained red, and mounted in glycerol acidified with 5 % H_2SO_4 (Soukup, 2014). Samples were observed using transmitted light (TBO and lignin) or fluorescence (CW; excitation at 355 nm, emission at 433 nm) microscopy (Olympus Provis AX 70).

Cell size and number analysis

Quantitative traits (cell and organ size, number of cell layers in hand sections, thickness of cotyledon, and cotyledon epidermal cells in semi-thin sections) were measured using NIS-Elements software (Laboratory Imaging, Praha, Czech Republic). For stem and cotyledon thickness and cotyledon epidermal cell thickness, sections were measured 5–10 times in various positions, and the mean value was calculated (Supplementary Data Fig. S2A, D, E). The thickness of the 5th true leaf was measured at the midrib position (Fig. S2B). Cell numbers of cotyledon semi-thin sections and stem hand sections were measured at several positions (marked with probes in Fig. S2F, G), and the mean value was calculated. At least four biological replicates were performed, and about ten plants for each variant were analysed in each biological replicate.

Cotyledon pavement cells area and circularity measurements

The circularity and area of pavement cells was assayed in mature cotyledons (14-d-old *in vitro*-grown plants) and mature 5th leaves (4-week-old plants grown in peat pellets). Leaves were stained in an aqueous solution of 1 µM FM4-64 dye for 2 h, and observed under the laser scanning microscope (Leica TCS SP2). The circularity and area were calculated with ImageJ software (http://rsb.info.nih.gov/ij/;tool: circularity measurement, area measurement) using the following equation:

$$f_{\text{circ}} = 4\pi A / p^2$$

where A stands for area and p for perimeter of the pavement cell. Approximately 300 cells in total from 25 plants were analysed in each variant.

Hypocotyl thickness and length measurement

Hypocotyl thickness and length were measured in 10-d-old etiolated plants grown *in vitro*. For hypocotyl thickness, seedlings were mounted on a microscopic slide and observed using transmitted light microscopy (Olympus Provis AX 70). Hypocotyl thickness was measured at the position of the 5th cell from the root–hypocotyl boundary using the ImageJ software length measurement tool (Fig. S2C). For hypocotyl length, seedlings were imaged using a Nikon D 3200 camera and length was measured using ImageJ software. Approximately 50 plants for each variant were analysed.

GUS histochemical staining

Cotyledons, mature leaves and hand microtome cross-sections of freshly harvested stems were incubated in 90 % ice cold acetone for 30 min and then washed twice in phosphate buffer (PB: 0.28 M KH_2PO_4, 0.72 M K_2HPO_4, pH 7.2) for 15 min. They were then incubated in GUS assay buffer (0.1 M $K_3[Fe(CN)_6]$, 0.1 M $K_4[Fe(CN)_6]$, 10 % Triton X-100, 2 mM 5-bromo-4-chloro-3-indoxyl-β-D-glucuronide in PB) at 37 °C until the sections were stained blue. The sections were then placed in 70 % ethanol and observed using an Olympus Provis AX 70 transmitted light microscope.

Local auxin application

Lanolin wax (Medela AG, Baar, Switzerland) was mixed with 100 mM naphthalene-1-acetic acid (NAA) dissolved in DMSO to achieve a final concentration of 1 mM NAA. For control treatments, lanolin was mixed with DMSO to achieve the final concentration of 1 % DMSO. Lanolin was applied to the base of 6-week-old DR5-GUS-expressing plants using a wooden stick. After 7 d, the stems were sectioned at the site of auxin application, and sections were subjected to GUS staining as described above.

AUX1-YFP confocal microscopy in sections

Hand sections 300 µm thick from the base inflorescence stems of 6-week-old AUX1-YFP and AUX1-YFP/*arpc5* plants were prepared, submerged in water and observed immediately under a Zeiss LSM 510 confocal microscope using Plan-Apochromat dry objective (20×, NA=0.8) or C-Apochromat water immersion objective (40×, NA=1.2). An argon 488 nm

laser was used for the excitation of fluorescence and the emission was recorded in the range 505–550 nm using a standard green fluorescent protein (GFP) filter set. The identity of the yellow fluorescent protein (YFP) fluorescence emission peak was independently verified for every image acquired using a spectral scan spanning the emission range 500–750 nm. The amount of AUX1-YFP fluorescence in plants used in experiments was monitored in 14-d-old plantlets before use in the experiment. Only plants showing AUX1-YFP in their root tips at a level comparable to the WT were used in the study (Supplementary Data, Fig. S3).

Auxin transport assay

^{3}H-NAA transport was measured in stem segments according to the original protocol of Okada *et al.* (1991), as described by Lewis and Muday (2009). Briefly, 2.5-cm inflorescence stem segments cut 2 cm from the apex of 6-week-old plants were immersed into 100 nM water solution of [^{3}H]NAA (specific radioactivity 20 Ci mmol^{-1}, American Radiolabeled Chemicals, ARC, Inc., St Louis, MO, USA) for 6 h. Each segment was cut into 5-mm sections, which were placed individually into the scintillation vials and extracted for 30 min with 96 % ethanol. After adding to the scintillation cocktail, vials were shaken for 20 min and radioactivity was immediately measured in a liquid scintillation counter (Packard Tri-Carb 2900TR, Packard Instrument Co., Meriden, CT, USA). Corresponding levels of ^{3}H-NAA in individual sections (expressed in pmol) were plotted as means (±s.d.) from three biological repetitions, each performed with 8–10 segments (plants). As a control, segments were immersed in ^{3}H-IAA in the opposite orientation, i.e. with their basal ends.

Carbohydrate analysis of stems and hypocotyls

The analyses of polysaccharides were performed on 4-d-old dark-grown hypocotyls and 6-week-old stems on an alcohol-insoluble residue (AIR) prepared as follows. In total, 100 mg (f. wt) of ground samples was washed twice in four volumes of absolute ethanol for 15 min, then rinsed twice in four volumes of acetone at room temperature for 10 min and left to dry in a fume hood overnight at room temperature.

The dry weight of samples was measured. After saponification of the AIR (10 mg) with 0.1 M NaOH, pectins were extracted from this pellet with 0.5 % ammonium oxalate at 80 °C for 2 h as described (Krupková *et al.*, 2007; Mouille *et al.*, 2007; Neumetzler *et al.*, 2012). Uronic acids were then quantified by colorimetry using the *m*-phenyl-phenol-sulfuric acid method as described (Nolen and Pollard, 2007).

The residual pellet was then used to determine the monosaccharide composition of the cell wall. Neutral monosaccharide composition was performed on 10 mg of AIR after hydrolysis in 2.5 M trifluoroacetic acid (TFA) for 1.5 h at 100 °C as described by Harholt *et al.* (2006). To determine the cellulose content, the residual pellet obtained after the TFA hydrolysis was rinsed twice with ten volumes of water and hydrolysed with H_2SO_4 as described by Updegraff (1969). The released glucose was diluted 500 times and then quantified using HPAEC-PAD chromatography as described previously (Harholt *et al.*, 2006; Krupková *et al.*, 2007; Mouille *et al.*, 2007).

RESULTS

Epidermal pavement cell shape and size defects are more pronounced in cotyledons than in mature leaves in ARP2/3 complex mutants

We have compared three lines of *Arabidopsis* carrying T-DNA insertions in the *ARP2*, *ARPC4* and *ARPC5* genes. In all three lines, mature leaves had distorted trichomes typical for the *distorted* group of mutants (Fig. 1A). Expression of *ARP2*, *ARPC4* and *ARPC5* was determined by qRT-PCR in *arp2*, *arpc4* and *arpc5* mutant homozygous lines (Fig. 1B). The amount of transcripts reaching background levels in all tested mutants suggests their knock-out character. In all three mutant lines, cotyledon epidermal pavement cells were less lobed (Fig. 1C), having significantly higher circularity (Fig. 1D) and cell area (Fig. 1E) when compared with WT plants. In contrast, the phenotype of decreased lobe formation was not detectable in 5th mature leaves of *arp2*, *arpc4* and *arpc5* mutants (Fig. 1F) and even significantly decreased circularity was observed here for the *arpc5* mutant. Fifth mature leaf pavement cell areas were significantly higher in *arpc4* and *arpc5* mutants (Fig. 1G). Cell–cell adhesion defects, demonstrated as gaps between epidermal cells, were observed in all mutants in cotyledons, as well as in 5th true leaves (Supplementary Data Fig. S4). Gaps were observed frequently between pavement cells, as well as pavement cells and stomatal guard cells in cotyledons (Fig. S4A, B). Gaps in mature leaves were observed exclusively to be adjacent to stomata (Fig. S4C, D).

These results suggest different ARP2/3-dependent epidermal cell morphogenesis in cotyledons and true leaves.

Radial thickness and elongation of above-ground organs is disturbed in ARP2/3 complex mutants

We have analysed changes in the thickness and length of the above-ground organs. A significant decrease of cotyledon thickness was detected only in the *arpc5* mutant (Fig. 2A). However, the thickness of the midrib region of the 5th mature leaf was significantly decreased in all tested mutants (Fig. 2B). Similarly, while the diameter of young (10-d-old) dark-grown hypocotyl was significantly decreased only in the *arpc4* mutant (Fig. 2C), the diameter of mature inflorescence stems was significantly decreased in all three mutants (Fig. 2D). In contrast, the length of both young dark-grown hypocotyls (Fig. 2E) and mature inflorescence stems (Fig. 2F) were decreased in all tested mutants.

Altogether, on the organ level, both hypocotyl and inflorescence stem elongation are disturbed in all three distorted mutants tested. Defects in organ thickness appear consistently in organs formed during post-embryonic development, perhaps because organ expansion is manifested primarily in older plants.

To understand how the epidermal layer contributes to the decreased thickness of cotyledon in the *arpc5* mutant, the number of all cell layers and average thickness of adaxial epidermis were analysed on semi-thin cotyledon transverse

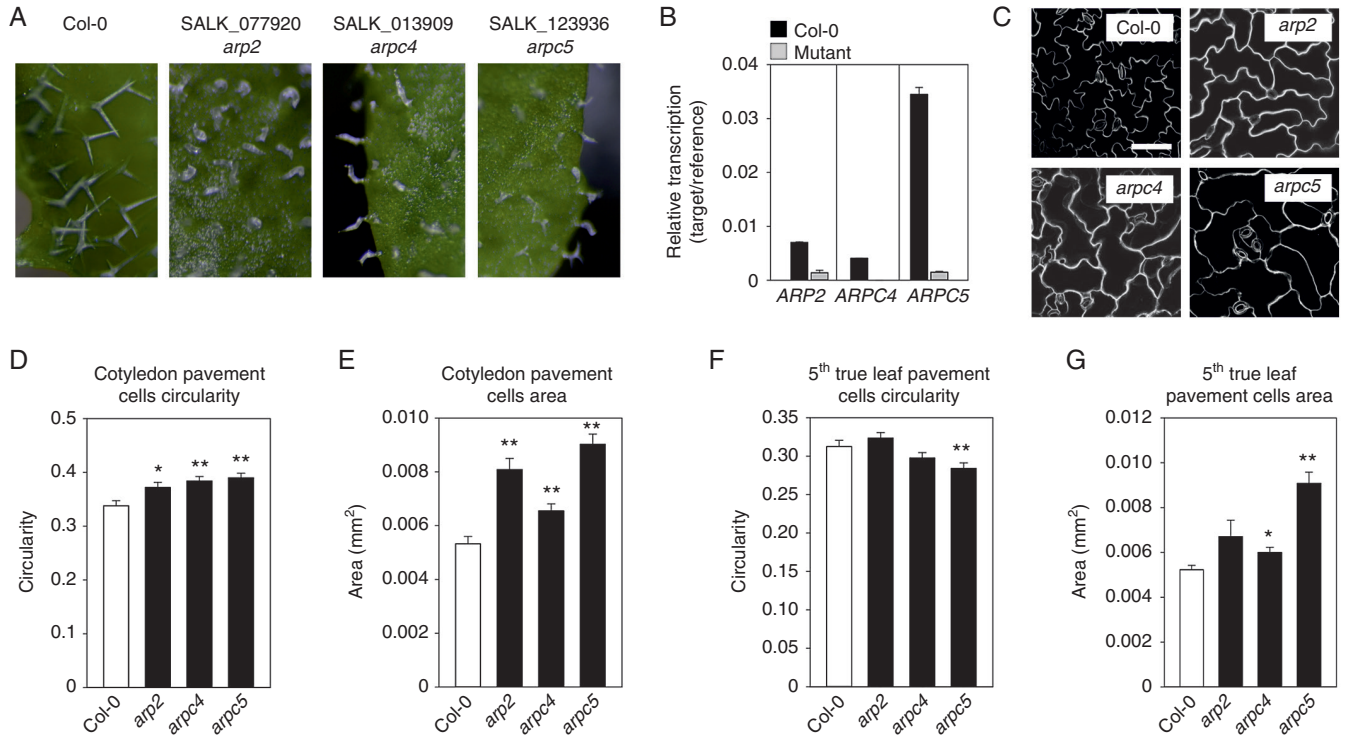

FIG. 1. Phenotype of *arp2*, *arpc4* and *arpc5* mutants. (A) All mutants display a similar phenotype, i.e. distorted swollen trichomes lacking pointed branches. (B) qRT-PCR showing knock-out character of mutation lacking respective transcript. Cotyledon pavement cells of all mutants visualized using FM4-64 dye (C) have increased circularity (D) and cell area (E). (F) Fifth true leaves pavement cells do not display increased circularity. (G) Increased cell area is detectable in *arpc4* and *arpc5* mutants. Scale bar (C) = 100 µm. $*P < 0.05$, $**P < 0.01$.

sections. As shown in Fig. 3A, the number of cell layers in all mutants was similar to that of the WT. Therefore, decreased cotyledon thickness in the *arpc5* mutant is not associated with the loss of cell layers. Interestingly, the adaxial epidermal layer was significantly thicker in *arp2* mutants, but *arpc4* and *arpc5* mutants were comparable to the WT (Fig. 3B). This suggests that in cotyledon, cells originating from layers other than adaxial epidermis must contribute to the decreased thickness of *arpc5* cotyledon. Cell layer counting in each 5th mature leaf was not possible due to the complex non-stratified structure of this tissue.

Analysis of the number of cell layers in inflorescence stems was performed across the whole radius of the stem, and separately in the interfascicular and cortex region (Fig. 3C). The number of cell layers decreased significantly when measured along the inflorescence stem radius, with approx. 25 cells for WT plants, and around 20 cells in mutants (Fig. 3D). This suggests that the loss of cells due to a lower number of periclinal divisions contributed to the decrease in inflorescence stem thickness in all mutants. It is possible that all tissues contributed to the loss of inflorescence cell layers; the interfascicular region, for example, also showed a decreased number of cell layers (Fig. 3F), albeit not significantly for *arp2* mutants. Similarly, the number of cortex cell layers was decreased for *arpc4* and *arpc5* mutants, although the difference was not statistically significant in *arpc4* mutants when compared to WT (Fig. 3H). The trend of cell layer loss was partially compensated for by cell volume growth, which is indicated by the greater cross-sectional area of interfascicular cells (Fig. 3G) and the thickness of inflorescence stem epidermis (Fig. 3E).

Therefore, various tissues within the inflorescence stem were affected in ARP2/3 mutants regarding loss of cell numbers, cell expansion and cell differentiation.

Cell wall thickness, lignification and cellulose content is changed in ARP2/3 complex mutants

Changes in tissue organization in the interfascicular layers of inflorescence stems of three mutants lacking the ARP2/3 complex suggested that cell wall composition could be changed in these tissues. Lignification occurs in xylem cells of vascular tissues as well as in interfascicular tissues. Therefore, we analysed cell wall thickness and lignification degree in inflorescence stem tissues. Phloroglucinol-HCl staining revealed reduced lignification in all three mutants, which was especially pronounced in interfascicular tissues (Fig. 4A–D). Interfascicular cell walls of the cells shown in Fig. 4A–D were significantly thinner in all three mutants (Fig. 4I). In contrast, phloem cap cells in mutants displayed extensive lignification, which was only rarely observed in WT (Fig. 4E–H, J).

We analysed the cell wall composition of etiolated hypocotyls and mature inflorescence stems. This did not reveal any changes in the cellulose, hemicellulose or ammonium oxalate-extracted homogalacturonan fraction content in etiolated hypocotyls (Fig. 5A, C, E). However, the cellulose content was decreased in inflorescence stems for all mutants tested when compared

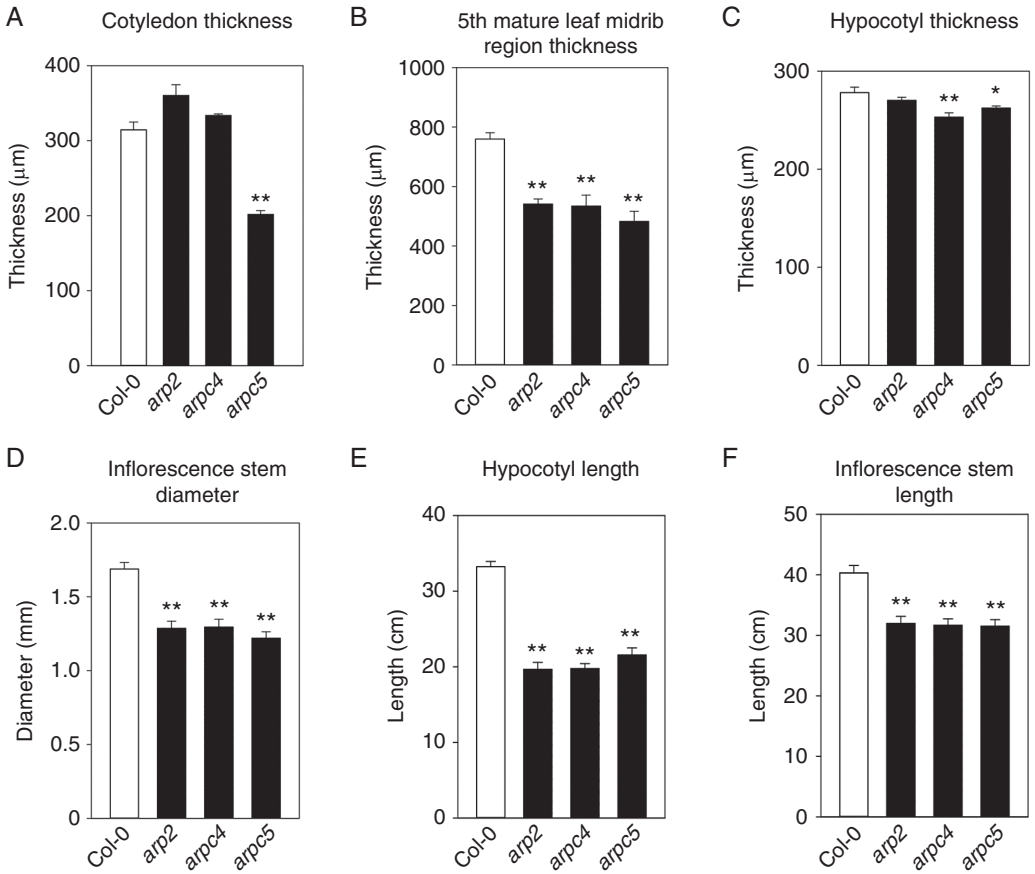

FIG. 2. Mature organs of ARP2/3 mutants are thinner. (A,B) Cotyledon thickness is decreased in *arpc5* (A), and mature 5th leaf thickness in the midrib region is lower in all mutants (B). (C,D) Hypocotyls of 14-d-old etiolated seedlings are thinner in *arpc4* and *arpc5* mutants (C), and inflorescence stem base of 6-week-old plants is thinner in all mutants (D). (E,F) Hypocotyls of 10-d-old etiolated seedlings (E) and inflorescence stems of 6-d-old plants (F) are significantly shorter for all mutants. $*P < 0.05$, $**P < 0.01$.

to WT, with a statistically insignificant difference for *arpc5* (Fig. 5B). The cellulose/hemicellulose ratio was increased in mutants (Fig. 5D), although the increase was not statistically significant for the *arp2* mutant. Finally, the homogalacturonan fraction was increased in all mutants, with the *arpc4* increase not statistically significant (Fig. 5F).

These results suggest specific changes in the cell wall composition occurring during post-embryonic development.

Auxin distribution is disrupted in ARP2/3 mutants

Since the above-mentioned phenotypes suggested changed morphogenesis of above-ground tissues in ARP2/3 mutants, an important morphogenic phytohormone, auxin, was tested for its involvement in these effects. To test if observed changes of tissue and cell organization in ARP2/3 mutants are associated with changes in the distribution and levels of auxin, *arpc5* mutants were crossed with the DR5::GUS marker line. Histochemical analysis of GUS expression in *in vitro* grown 7-d-old cotyledons revealed that in DR5::GUS plants, cotyledons contained DR5 signal along the vasculature, but this signal was decreased in DR5::GUS/*arpc5* mutants (Fig. 6A, B). Importantly, this effect was restricted only to the early stages of cotyledon development. The difference between WT and mutant plants was gradually abolished during further development, as documented for *ex vitro* growing cotyledons after 11 and 14 d (Supplementary Data Fig. S5). Similarly, the amount of GUS in the inflorescence base stem cross-sections did not show any difference between DR5::GUS and DR5::GUS/*arpc5* plants (Fig. 6C, D).

To further test the response of mature *arpc5* tissues to auxin, NAA was applied locally to the inflorescence stem base of 6-week-old plants. After 7 d, cross-sections were analysed for the amount of GUS. This local external auxin application resulted in high GUS expression in control DR5::GUS plants with GUS being strongly upregulated in both xylem and phloem vascular poles and even in the pith (Fig. 6E). In contrast, mutant DR5::GUS/*arpc5* plants responded only mildly (Fig. 6F) in the inner tissues, suggesting reduced lateral permeability or the distribution of auxin between tissues in general. In this process, the importance of the major auxin influx carrier AUX1 being localized in the inflorescence stem procambial and protoxylem cells has been documented for overall stem development. Quadruple mutants lacking all auxin influx carriers *aux1/lax1/lax2/lax3* display similarities to the ARP2/3 mutants tested in our work, namely in the disturbed organization of vascular tissues and reduction of inflorescence stem diameter (Fabregas *et al.*, 2015). To follow the distribution of AUX1 in *arpc5*, a marker line expressing AUX1::AUX1:YFP was crossed with an

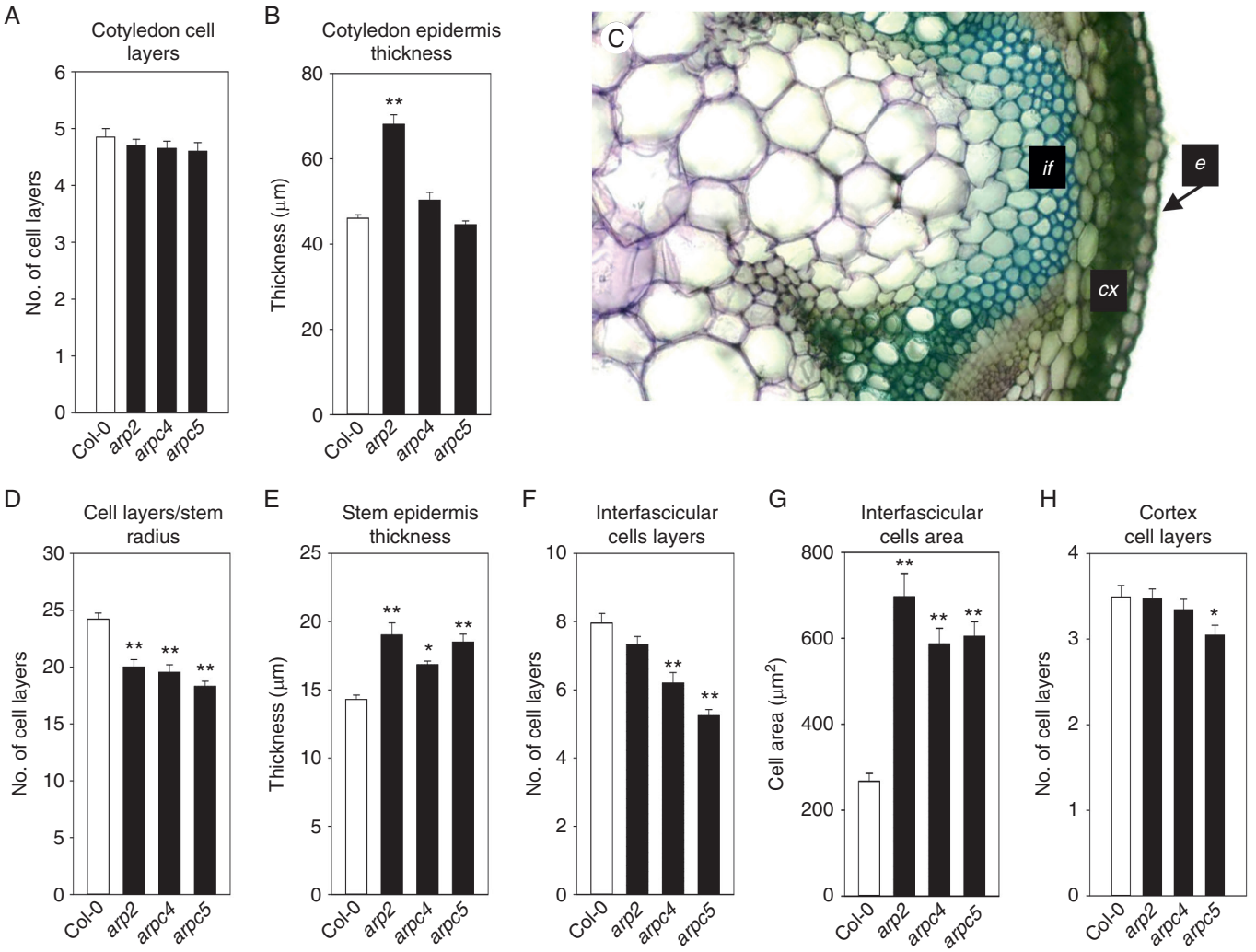

FIG. 3. Loss of cell layers and cell size changes in ARP2/3 mutants. (A,B) Transverse sections of 14-d-old cotyledons were used to analyse cell layer number and size. The number of cell layers in the cotyledon is not changed (A), while the thickness of the epidermal cell layer is increased in the *arp2* mutant, but not in *arpc4* and *arpc5* mutants (B). (C) Hand sections of the inflorescence stem base of 6- to 7-week-old plants were used to analyse cell layer numbers and sizes in the cortex (cx), interfascicular region (if) and epidermis (e). (D) The number of cells per inflorescence stem radius decreased in all ARP2/3 mutants tested. (E) Stem epidermal cells are significantly thicker in all mutants tested. (F) The number of interfascicular cell layers is significantly lower in *arpc4* and *arpc5* plants, while the decrease is not significant in *arp2* mutants. (G) Interfascicular cell area is significantly increased in inflorescence stems of all mutants. (H) The number of cortex cell layers is not significantly changed in ARP2/3 mutants. Toluidine blue staining (C). $*P < 0.05$, $**P < 0.01$.

arpc5 mutant. Confocal microscopy of fresh hand sections of inflorescence stems revealed that AUX1:YFP was localized in procambial and protoxylem cells in control AUX1::AUX1:YFP plants (Fig. 6G), but AUX1::AUX1:YFP/*arpc5* had greatly reduced signal, suggesting much lower abundance of AUX1 in the provascular tissues in the *arpc5* mutant (Fig. 6H). This indirectly suggests a decreased ability of ARP2/3 mutants to generate auxin maxima needed for vasculature development. However, this might also influence overall basipetal transport of auxin in the inflorescence stem. To test how all studied ARP2/3 mutants (*arp2*, *arpc4* and *arpc5*) transport auxin in the basipetal direction, auxin transport assays were performed in the inflorescence stem segments. As shown in Fig. 6I, the application of ^{3}H-NAA, a synthetic auxin primarily marking the activity of auxin efflux carriers (Delbarre *et al.*, 1996; Parry *et al.*, 2001), for 6 h to the apical part of WT inflorescence stems resulted in its transport through the tissue and the accumulation in the last segment 15–25 mm from the application point. In contrast, the majority of applied ^{3}H-NAA accumulated in the first segment of all three mutants, suggesting reduced basipetal transport of auxin through their inflorescence stems (Fig. 6I). The transport of ^{3}H-NAA was almost negligible when measured in inverted segments (Supplementary Data Fig. S5).

DISCUSSION

Epidermis-related ARP2/3 phenotypes are manifested differently in cotyledons and mature leaves

Here we show that three independent ARP2/3 mutants, *arp2* (Djakovic *et al.*, 2006), *arpc4* (SALK_013909) and *arpc5* (Li *et al.*, 2003), have analogous phenotypes, which can be thus associated with the loss of ARP2/3 complex function. Phenotypes

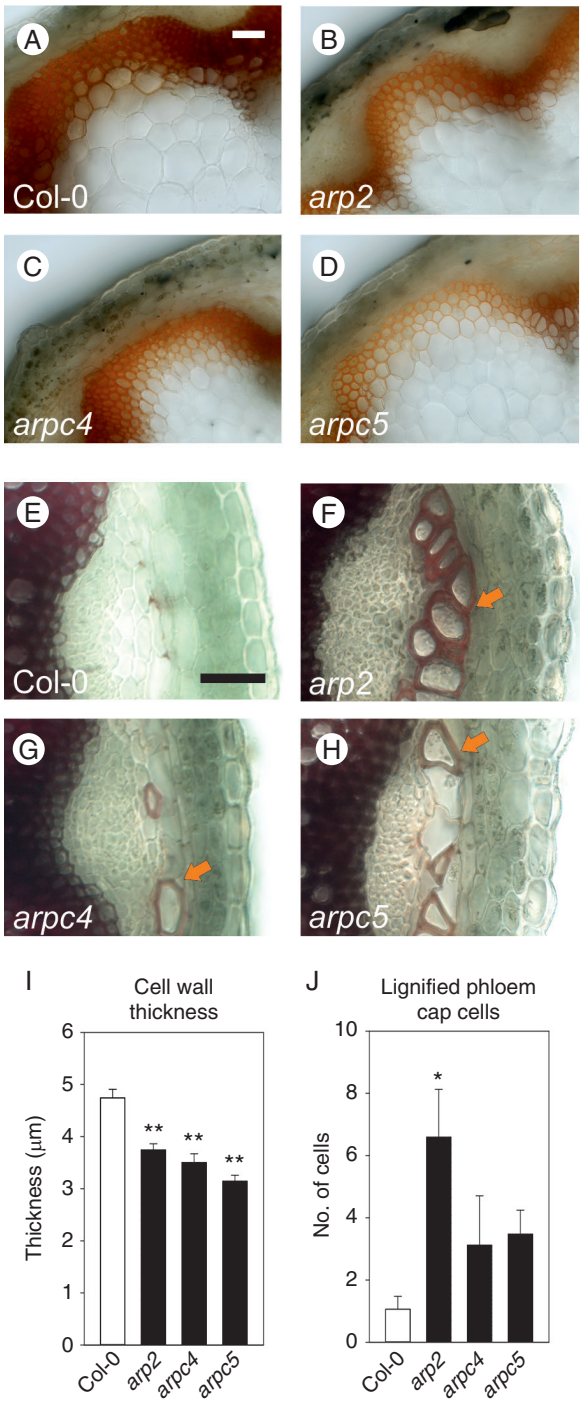

FIG. 4. Thickness of the cell wall and lignification is altered in ARP2/3 mutants. (A–D) Phloroglucinol HCl staining of transverse sections through the base of the inflorescence stems. Lignification level of interfascicular cells and vascular bundles of *arp2* (B), *arpc4* (C) and *arpc5* (D) mutants is decreased when compared to WT (A). (I) Lignified cell walls in interfascicular tissue shown in A–D are thinner. (E,H,J) In contrast, all mutant plants show increased deposition of lignin in the phloem fibre cells of the phloem cap. Whereas only a few lignified phloem fibre cells per vascular bundle are detectable in WT plants (E, J), a significantly increased number of lignified phloem fibre cells is deposited in the *arp2* mutant (F, J). Non-significant increases in the number of lignified phloem fibre cells was detected in *arpc4* (G, J) and *arpc5* (H, J) mutants. Arrows in F–H indicate lignified phloem fibre cells. Scale bar = 50 µm (A-H). $*P < 0.05$, $**P < 0.01$.

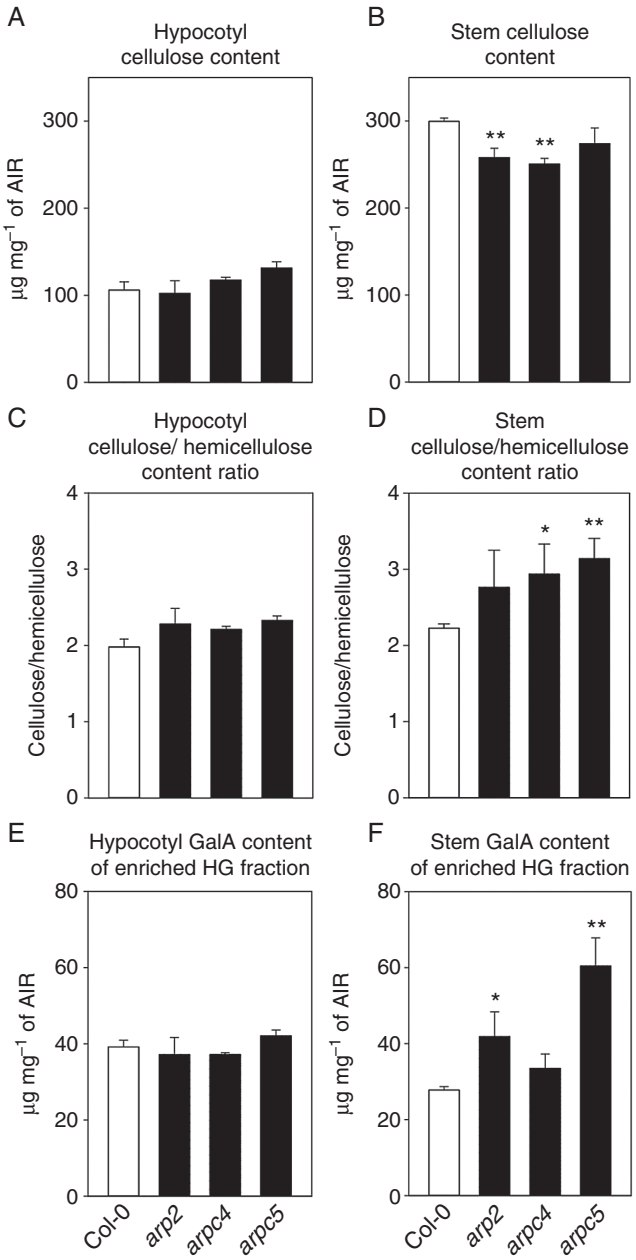

FIG. 5. Cell wall composition is altered in ARP2/3 mutants. (A–F) Cell wall was isolated from 4-d-old etiolated hypocotyls (A, C, E) and 6-week-old inflorescence stems (B, D, F), and the composition of the cell wall was analysed. The cellulose content is not changed in hypocotyls (A), but decreased in mature inflorescence stems in ARP2/3 mutants, with statistically significant decreases for *arp2* and *arpc4* mutants (B). Similarly, cellulose/hemicellulose ratio is not changed in hypocotyls (C), but decreased in mature inflorescence stems, with statistically significant increases for *arpc4* and *arpc5* (D). Galacturonic acid (GalA) content in ammonium oxalate fraction enriched in homogalacturonan (HG) is not changed in hypocotyls (E), but is increased in mature inflorescence stems, with statistically significant increases for *arpc4* and *arpc5* (F). $*P < 0.05$, $**P < 0.01$. AIR: alcohol-insoluble residue.

previously reported with the ARP2/3 complex mutants are increased circularity of cotyledon epidermal cells (Le *et al.*, 2003; Mathur *et al.*, 2003*a*, *b*; Saedler *et al.*, 2004*a*), gaps between epidermal cells in cotyledons (Le *et al.*, 2003; Mathur *et al.*, 2003*a*, *b*; El-Assal *et al.*, 2004*a*, *b*; Kotchoni *et al.*, 2009; Zhang *et al.*,

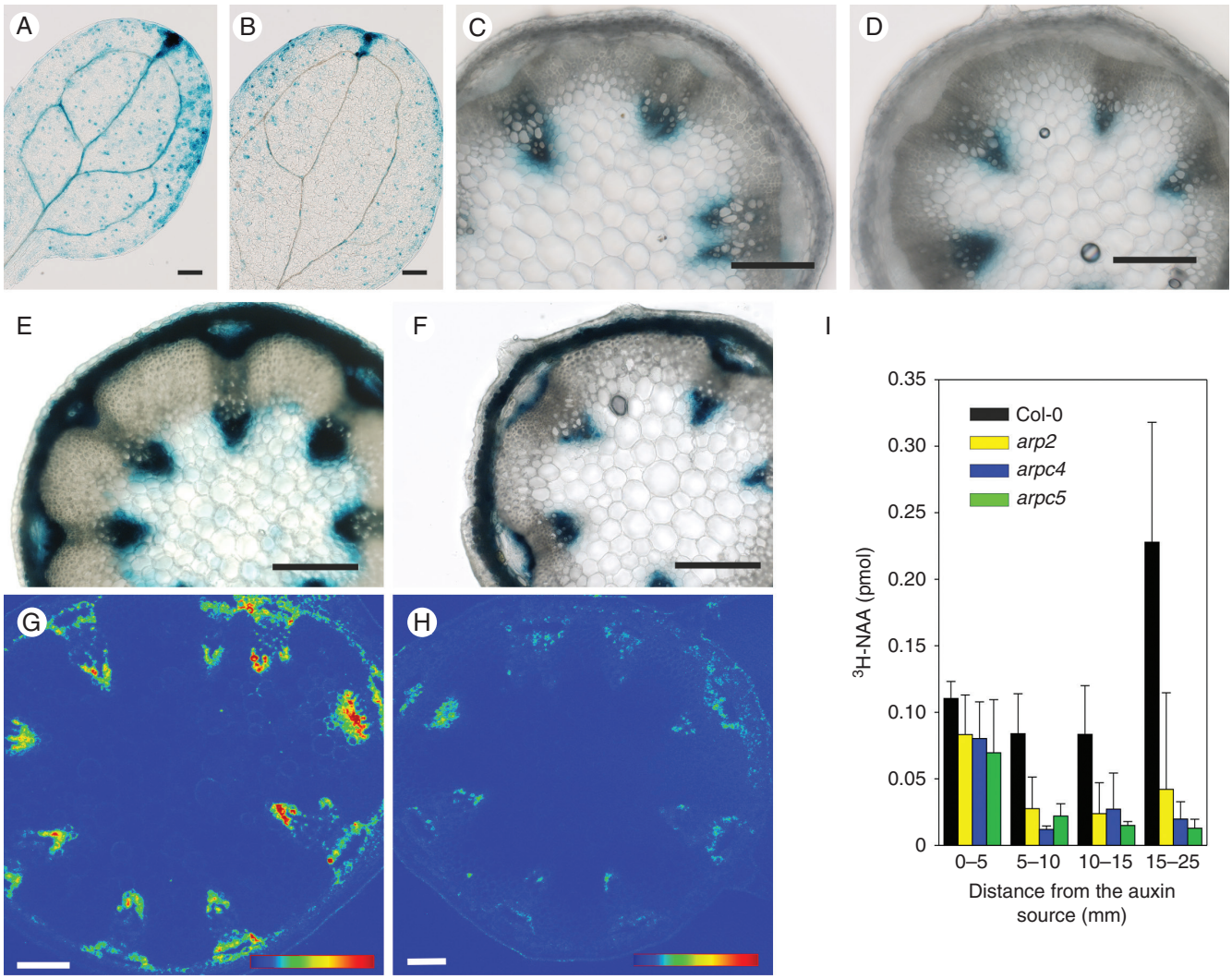

FIG. 6. Auxin-driven gene expression, transport and AUX1-YFP levels are reduced in ARP2/3 mutants. (A,B) GUS staining of 7-d-old cotyledons of DR5::GUS control seedlings (A) and DR5:.GUS/*arpc5* seedlings (B) showing patchy and less vasculature-associated auxin response in *arpc5* mutant plants. (C,D) GUS staining of 6-week-old inflorescence stem base section of DR5::GUS control plants (C) and DR5:.GUS/*arpc5* plants (D) localized at both phloem and xylem poles of vascular bundles. (E,F) External application of lanolin with 1 mM NAA to the inflorescence stem base 8 d before the sectioning inducing strong DR5::GUS expression in the control WT stem especially at both phloem and xylem poles (E), but milder expression in the *arpc5* mutant (F). Single confocal section through the inflorescence stem base sections of AUX1::AUX1:YFP plants (G) and AUX1::AUX1:YFP/*arpc5* (H) with reduced AUX1-YFP signal in *arpc5* plants. Scale bar = 200 µm (A–F) and 100 µm (G, H). In G and H, 8-bit LUT bar represents the grey range between 0 and 255 (0 blue, 70 green, 140 yellow, 210 red). (I) Auxin transport assays in inflorescence stem segments isolated from the apical part of cut inflorescence stems of WT and *arp2*, *arpc4* and *arpc5* plants. Note reduced basipetal transport of ^{3}H-NAA through inflorescence stem in all three mutants. Scale bar = 200 µm.

2013*b*), distorted trichomes in true leaves (Mathur *et al.*, 1999; Szymanski *et al.*, 1999; Li *et al.*, 2003; Le *et al.*, 2003; Schwab *et al.*, 2003; Basu *et al.*, 2004, 2005; El-Assal *et al.*, 2004*a*, *b*), stomata movements (Li *et al.*, 2014), reduced hypocotyl length (Dyachok *et al.*, 2011) and reduced plant weight (Le *et al.*, 2003).

The analysis revealed that some phenotypes of mutants lacking the ARP2/3 complex were no longer detectable in pavement cells of 5th mature true leaves. For example, a strong increase in area of pavement cells in cotyledons was not noticed consistently in the mutant 5th true leaves. Importantly, increased circularity of cotyledon pavement cells was not further manifested at all in true leaves in any of the tested mutants. This suggests that phenotypic manifestation of ARP2/3 complex loss may be overridden by other cell shape-controlling processes in true leaves, such as mechanical forces (Sampathkumar *et al.*, 2014), or the ROP signalling cascade (Fu *et al.*, 2002, 2005; Basu *et al.*, 2008). Interestingly, SPIKE1 was shown to interact with ROP GTPase proteins (Basu *et al.*, 2008; Ren *et al.*, 2016), thus providing a possible link between the ROP signalling pathway and ARP2/3-controlled actin reorganization (Basu *et al.*, 2008). However, our results suggest differential involvement of the ARP2/3 complex in cell shape control in cotyledons and true leaves, with rather negligible involvement of the ARP2/3 complex in pavement cell lobe formation in mature leaves.

In contrast to the cell shape defect, cell–cell adhesion defects were found in both cotyledons and true leaves. Similarly, distorted trichomes could be detected in all true leaves as well as in other organs. These defects seem to be the result of the disruption of a general pathway or process controlled by ARP2/3-nucleated actin cytoskeleton, as discussed hereinafter.

Loss of ARP2/3 complex results in radial growth and elongation defects in above-ground mature tissues

All three mutants consistently displayed defects in organ radial expansion, where tissues formed during post-embryonic development were clearly more affected than tissues in young seedlings. For example, cotyledon thickness was significantly decreased only for one mutant, but all mutants displayed significantly thinner true leaves. Similarly, hypocotyl thickness was not consistently decreased in all mutants, but inflorescence stems were significantly thinner in all mutants tested.

A stunted hypocotyl phenotype was reported for ARP2/3 mutants (Mathur *et al.*, 2003*b*; Basu *et al.*, 2004, 2005; El-Assal *et al.*, 2004*b*; Li *et al.*, 2004; Saedler *et al.*, 2004*b*; Le *et al.*, 2006; Zhang *et al.*, 2008). Here we show that a stunted hypocotyl phenotype was accompanied by only a mild decrease in hypocotyl thickness, which further suggests defects in cell elongation rather than radial cell expansion. Due to regular organization of inflorescence stem tissues, we were able to closely analyse the cell structure changes in stem transverse sections to determine if the decreased thickness was due to the loss of cell layers, or decreased size of cells. Surprisingly, the loss of cell layers, which tended to affect all tissues within the inflorescence stem, was accompanied by generally increased expansion of individual cells (measured for epidermal and interfascicular region) in mutants. The radial component of volume growth was particularly enhanced in the interfascicular region. Therefore, the reduced thickness of mutant stems caused by a lower number of periclinal divisions resulting in a lower number of cell layers was partially compensated for by increased cell expansion.

ARP2/3 determines cell wall composition

Increased cell size in ARP2/3 mutants was accompanied by thinner cell walls and reduced lignin content in interfascicular tissues. Indeed, the first report on the localization of ARP2/3 subunits in plants localized the activity of the *ARP2* promoter to the close proximity of xylem vessels, typical lignin-deposition types of cells (Klahre and Chua, 1999). The cell walls of mature tissues showed decreased cellulose content and increased homogalacturonan fraction content, which was accompanied by the phenotype of thinner organs. Interestingly, reduced cellulose content was detectable also in actin isotype mutants (Sampathkumar *et al.*, 2013), but with the phenotype clearly detectable already in the young seedling stage. Thinner cell walls, reduced cellulose content, increased homogalacturonan fraction content and reduced lignification in ARP2/3 complex mutants probably decreased further mechanical properties of the whole inflorescence stem, resulting in lower plant height and lignification of phloem cap as a possible compensatory mechanism. Note that we did not observe ectopic lignification in ARP2/3 mutants, which has been observed to accompany cellulose deficiency (Desprez *et al.*, 2002; Cano-Delgado *et al.*, 2003; Bischoff *et al.*, 2009; Brabham *et al.*, 2014).

Most phenotypes reported previously in ARP2/3 complex mutants, as well as new phenotypes described in this work (thinner mature organs and reduced plant height), may be associated with defects in cell wall building. For example, the phenotype of distorted trichomes is caused by abnormal deposition of the cell wall material during trichome growth (Yanagisawa *et al.*, 2015). Furthermore, cell–cell adhesion defects are reported for mutants with altered cell wall composition, such as *quasimodo2* (Bouton *et al.*, 2002; Mouille *et al.*, 2007). However, *quasimodo2* mutants show rather strong phenotypes such as plant dwarfism associated with decreased pectin content detectable even in the earliest stages of development (Mouille *et al.*, 2007), which was not observed in ARP2/3 mutants. Although cell–cell adhesion defects in ARP2/3 mutants are probably related to cell wall changes, the exact mechanism of their origin needs further explanation.

Abnormal deposition of cell wall material in the cell corners of the root tip and reduced rigidity of roots was observed also by Dyachok *et al.* (2008). However, the chemical composition of the root cell wall of 5-d-old seedlings was unchanged in ARP2/3 mutants (Qiu *et al.*, 2002; Dyachok *et al.*, 2008). Our analysis of mutant seedlings confirmed these results. Hypocotyl cell walls did not reveal any changes in cellulose content, hemicellulose content or homogalacturonan fraction. We were also not able to detect any changes through Fourier-transform infrared analysis of hypocotyl cell walls (data not shown). We concluded that cell wall composition changes became prominent later, during post-embryonic development. Stunted hypocotyl length has been reported repeatedly for ARP2/3 mutants. Although this phenotype may be associated with problems also in cell wall synthesis, our data on the rather unchanged diameter of hypocotyls, as well as unchanged carbohydrate composition and structure of the cell wall suggest the involvement of other mechanisms, such as the disturbed light signalization that was reported for roots of ARP2/3 mutants (Dyachok *et al.*, 2011).

Carrier-mediated auxin transport involving both auxin influx and efflux is reduced in ARP2/3 mutants

The phenotype of thin cell walls, increased cell volumes of interfascicular tissues, decreased lignification and altered development prompted us to analyse the level of auxin. Indeed, cell wall quality modulates auxin transport through plant tissues, which is informative for plant development (Braybrook and Peaucelle, 2013; Paque *et al.*, 2014; Pitaksaringkarn *et al.*, 2014; Xu *et al.*, 2014). Here we show that the phenotype of ARP2/3 complex mutants is accompanied by decreased auxin maxima in cotyledons, and reduced lateral distribution and basipetal auxin transport as well as decreased expression of auxin transporter AUX1 in stems. There are two possible explanations for our observations: they are based either on the potential role of the ARP2/3 complex in controlling intracellular trafficking processes in cells and tissues needed for targeted deposition of cell wall components, or on integral and peripheral plasma membrane proteins involved in auxin transport.

There is no doubt that the actin cytoskeleton participates in cell wall synthesis (Kandasamy *et al.*, 2009; Sampathkumar *et al.*, 2013). On the other hand, the ARP2/3 complex may function in more specific aspects of actin-controlled cell wall building processes, such as delivery of cell wall material for specialized cell

walls in tips of root hairs, trichomes and plasmodesmata (Van Gestel *et al.*, 2003; Qiu *et al.*, 2015; Yanagisawa *et al.*, 2015). Trichomes represent an example of such a specialized cell. The mechanism behind formation of distorted trichomes in mutants lacking the ARP2/3 complex was shown to be the disturbed transport of cell wall material (Yanagisawa *et al.*, 2015). The need for ARP2/3-controlled specialized cell wall deposition probably increases during plant maturation, when increased mechanical properties of the cell wall are needed to support expanding tissues. This could explain the cell wall phenotype observed in mature ARP2/3 mutants, but not in mutant seedlings. Since mutual interactions between the cell wall and auxin have been described recently, it is reasonable to link cell wall changes and auxin transport defects observed in ARP2/3 complex mutants. The observation that the *wat1* mutant lacking a vacuolar auxin transporter has thin cell walls and low lignification in later stages of plant development (Ranocha *et al.*, 2010, 2013) further justifies the idea of a cell wall–auxin interaction in ARP2/3 mutants. The quality of the cell wall is perceived by the cell and influences auxin homeostasis. Since localization of the auxin efflux carrier PIN1 was shown to be dependent on the stiffness of the cell wall (Braybrook and Peaucelle, 2013), changes in the quality of the cell wall of ARP2/3 mutants might be translated into the localization and function of molecules involved in auxin transport. On the other hand, our data indicate that auxin transport and accumulation defects were detectable as early as in the stage of cotyledon development. Changes to the cell wall composition detectable only later during post-embryonic development support the hypothesis that ARP2/3-dependent auxin transport defects are upstream of cell wall and differentiation defects in the mutants studied here. Note that auxin maxima in root tips of 14-d-old seedlings were not reduced in mutants, and that auxin distribution in roots in later developmental stages was not investigated in our study. Therefore, it needs to be determined if ARP2/3-related changes in the cell wall structure and auxin distribution are manifested specifically in aerial tissues of *Arabidopsis thaliana*, or if the ARP2/3 complex fulfils similar roles in roots as well.

The ARP2/3 complex has been localized to various organelles in plant cells (Zhang *et al.*, 2013*a, b*; Havelkova *et al.*, 2015). ARP2/3 complex subunit ARPC2 was shown to interact with cortical microtubules (Havelkova *et al.*, 2015). Recently, NAP1 was demonstrated to localize to autophagosomes (Wang *et al.*, 2016). Localization studies thus suggest that the ARP2/3 complex may be involved in the delivery and recycling of plasma membrane-localized auxin transporters, resulting in reduced auxin transport. Reduced auxin flow through tissues would then affect cell wall thickness and lignification, mainly through the regulated expression of auxin-responsive genes, including genes for auxin influx and efflux carriers (Ranocha *et al.*, 2013). Reduced inflorescence stem basipetal transport of NAA detected in all tested ARP2/3 mutants strongly suggests involvement of the PIN1 auxin efflux carrier, which may either wrongly localize, or have its expression compromised. However, *pin1* mutant plants usually have higher xylem differentiation, which is stimulated by accumulated auxin that cannot be dragged away from the sites of its synthesis (Galweiler *et al.*, 1998). In contrast, a close inspection revealed levels of AUX1 were impaired in ARP2/3 mutants. This is supported by impaired xylem differentiation previously shown in auxin influx carrier mutants (Fabregas *et al.*, 2015). Our results showing reduced lateral distribution of auxin also suggest that the ARP2/3 complex might be involved in the localization of PIN3, 4 and 7 and, therefore, in carrier-mediated lateral auxin permeability, recently described by Bennett *et al.* (2016) and Zou *et al.* (2016).

CONCLUSION

We show here that three independent lines lacking various ARP2/3 subunits show similar phenotypes, which are especially pronounced later during post-embryonic development. Morphological changes include thin organs and thin cell walls. Cell walls of inflorescence stems have reduced cellulose and increased homogalacturonan content. Auxin transport is reduced in all three ARP2/3 mutants tested in this study. The auxin influx carrier AUX1 shows changed expression pattern in stems and auxin maxima are reduced in *arpc5* mutants. We suggest that the plant ARP2/3 complex plays a morphogenetic role through the control of cell wall synthesis and/or auxin transport.

SUPPLEMENTARY DATA

Supplementary data are available at https://academic.oup.com/aob and consist of the following. Fig. S1: Col-0 plants and mutant lines SALK_077920.56.00 (*arp2*), SALK_013909.27.65 (*aprc4*) and SALK_123936.41.55 (*arpc5*) were obtained from the NASC T-DNA mutant collection (Scholl *et al.*, 2000). The homozygous state of the T-DNA insertion was confirmed by genotyping using the listed primers. Fig. S2: (A–D) Thickness measurements of (A) cotyledons using semi-thin sections, (B) midrib region (arrows) of the fully expanded 5th true leaves using hand sections, (C) hypocotyl thickness and (D) inflorescence stem thickness using hand sections. Fig. S3: The level of AUX1:YFP expression in stems of 6-week-old plants used in our study (Fig. 6G, H) was monitored in 14-d-old plantlets. *In vitro*-grown 14-d-old plants were carefully placed on a microscopic slide and root tips were analysed by fluorescence microscopy. Fig. S4: Quantification of cell adhesion defects in cotyledons and 5th true leaves. Leaves were stained in aqueous solution of 1 μM FM4-64 dye for 2 h, and observed under the laser scanning microscope (Leica TCS SP2). Fig. S5: (A–D) Histochemical analysis of GUS expression in cotyledons of 11- and 14-d-old plants expressing DR5::GUS marker. (A) Eleven-day-old WT plants have strong DR5::GUS signal in cotyledons. (B) This signal is reduced in *arpc5* plants expressing DR5::GUS. (C, D) Fourteen-day-old WT and *arpc5* plants have comparable auxin maxima in cotyledons.

ACKNOWLEDGEMENTS

We thank Dr Kelly Hennessey for manuscript proofreading, and the referees for their helpful comments during the submission process. This project was supported by NPU I, LO1417 (Ministry of Education, Youth and Sports of the Czech Republic), and Charles University Grant Agency, project No. 1604214. Microscopy was performed in the IEB image facility (CzBI LM2015062) and in the Laboratory of Confocal and Fluorescence Microscopy co-financed by the European Regional

Development Fund and the state budget of the Czech Republic, project nos. CZ.1.05/4.1.00/16.0347 and CZ.2.16/3.1.00/21515.

LITERATURE CITED

Baluška F, **Salaj J**, **Mathur J**, ***et al.* 2000**. Root hair formation: f-actin-dependent tip growth is initiated by local assembly of profilin-supported f-actin meshworks accumulated within expansin-enriched bulges. *Developmental Biology* **227**: 618–632.

Baluska F, **Jasik J**, **Edelmann HG**, **Salajova T**, **Volkmann D. 2001**. Latrunculin B-induced plant dwarfism: Plant cell elongation is F-actin-dependent. *Developmental Biology* **231**: 113–124.

Barbez E, **Dünser K**, **Gaidora A**, **Lendl T**, **Busch W. 2017**. Auxin steers root cell expansion via apoplastic pH regulation in *Arabidopsis thaliana*. *Proceedings of the National Academy of Sciences* **114**: E4884–E4893.

Basu D, **El-Assal SED**, **Le J**, **Mallery EL**, **Szymanski DB. 2004**. Interchangeable functions of Arabidopsis PIROGI and the human WAVE complex subunit SRA1 during leaf epidermal development. *Development* **131**: 4345–4355.

Basu D, **Le J**, **El Essal SED**, ***et al.* 2005**. DISTORTED3/SCAR2 is a putative arabidopsis WAVE complex subunit that activates the Arp2/3 complex and is required for epidermal morphogenesis. *Plant Cell* **17**: 502–524.

Basu D, **Le J**, **Zakharova T**, **Mallery EL**, **Szymanski DB. 2008**. A SPIKE1 signaling complex controls actin-dependent cell morphogenesis through the heteromeric WAVE and ARP2/3 complexes. *Proceedings of the National Academy of Sciences of the United States of America* **105**: 4044–4049.

Bennett T, **Hines G**, **van Rongen M**, ***et al.* 2016**. Connective auxin transport in the shoot facilitates communication between shoot apices. *Plos Biology* **14**: e1002446.

Bischoff V, **Cookson SJ**, **Wu S**, **Scheible WR. 2009**. Thaxtomin A affects CESA-complex density, expression of cell wall genes, cell wall composition, and causes ectopic lignification in *Arabidopsis thaliana* seedlings. *Journal of Experimental Botany* **60**: 955–965.

Bouton S, **Leboeuf E**, **Mouille G**, ***et al.* 2002**. Quasimodo1 encodes a putative membrane-bound glycosyltransferase required for normal pectin synthesis and cell adhesion in Arabidopsis. *Plant Cell* **14**: 2577–2590.

Brabham C, **Lei L**, **Gu Y**, **Stork J**, **Barrett M**, **Debolt S. 2014**. Indaziflam herbicidal action: a potent cellulose biosynthesis inhibitor. *Plant Physiology* **166**: 1177.

Braybrook SA, **Peaucelle A. 2013**. Mechano-chemical aspects of organ formation in *Arabidopsis thaliana*: the relationship between auxin and pectin. *Plos One* **8**: e57813.

Cano-Delgado A, **Penfield S**, **Smith C**, **Catley M**, **Bevan M. 2003**. Reduced cellulose synthesis invokes lignification and defense responses in *Arabidopsis thaliana*. *Plant Journal* **34**: 351–362.

Cosgrove DJ. 2005. Growth of the plant cell wall. *Nature Reviews. Molecular Cell Biology* **6**: 850–861.

Delbarre A, **Muller P**, **Imhoff V**, **Guern J. 1996**. Comparison of mechanisms controlling uptake and accumulation of 2,4-dichlorophenoxy acetic acid, naphthalene-1-acetic acid, and indole-3-acetic acid in suspension-cultured tobacco cells. *Planta* **198**: 532–541.

Desprez T, **Vernhettes S**, **Fagard M**, ***et al.* 2002**. Resistance against herbicide isoxaben and cellulose deficiency caused by distinct mutations in same cellulose synthase isoform CESA6. *Plant Physiology* **128**: 482–490.

Djakovic S, **Dyachok J**, **Burke M**, **Frank MJ**, **Smith LG. 2006**. BRICK1/HSPC300 functions with SCAR and the ARP2/3 complex to regulate epidermal cell shape in Arabidopsis. *Development* **133**: 1091–1100.

Durst S, **Nick P**, **Maisch J. 2013**. *Nicotiana tabacum* actin-depolymerizing factor 2 is involved in actin-driven, auxin-dependent patterning. *Journal of Plant Physiology* **170**: 1057–1066.

Dyachok J, **Shao MR**, **Vaughn K**, ***et al.* 2008**. Plasma membrane-associated SCAR complex subunits promote cortical F-actin accumulation and normal growth characteristics in Arabidopsis roots. *Molecular Plant* **1**: 990–1006.

Dyachok J, **Zhu L**, **Liao FQ**, **He J**, **Huq E**, **Blancaflor EB. 2011**. SCAR mediates light-induced root elongation in Arabidopsis through photoreceptors and proteasomes. *Plant Cell* **23**: 3610–3626.

Eggenberger K, **Sanyal P**, **Hundt S**, **Wadhwani P**, **Ulrich AS**, **Nick P. 2017**. Challenge integrity: the cell-penetrating peptide BP100 interferes with the auxin-actin oscillator. *Plant and Cell Physiology* **58**: 71–85.

El-Assal SED, **Le J**, **Basu D**, **Mallery EL**, **Szymanski DB. 2004***a*. Distorted2 encodes an ARPC2 subunit of the putative Arabidopsis ARP2/3 complex. *Plant Journal* **38**: 526–538.

El-Assal SE-D, **Le J**, **Basu D**, **Mallery EL**, **Szymanski DB. 2004***b*. Arabidopsis GNARLED encodes a NAP125 homolog that positively regulates ARP2/3. *Current Biology* **14**: 1405–1409.

Fabregas N, **Formosa-Jordan P**, **Confraria A**, ***et al.* 2015**. Auxin influx carriers control vascular patterning and xylem differentiation in *Arabidopsis thaliana*. *Plos Genetics* **11**: e1005183.

Fendrych M, **Leung J**, **Friml J. 2016**. TIR1/AFB-Aux/IAA auxin perception mediates rapid cell wall acidification and growth of Arabidopsis hypocotyls. *Elife* **5**: e19048.

Feraru E, **Feraru MI**, **Kleine-Vehn J**, ***et al.* 2011**. PIN polarity maintenance by the cell wall in Arabidopsis. *Current Biology* **21**: 338–343.

Fu Y, **Li H**, **Yang ZB. 2002**. The ROP2 GTPase controls the formation of cortical fine F-actin and the early phase of directional cell expansion during Arabidopsis organogenesis. *Plant Cell* **14**: 777–794.

Fu Y, **Gu Y**, **Zheng ZL**, **Wasteneys G**, **Yang ZB. 2005**. Arabidopsis interdigitating cell growth requires two antagonistic pathways with opposing action on cell morphogenesis. *Cell* **120**: 687–700.

Galweiler L, **Guan CH**, **Muller A**, ***et al.* 1998**. Regulation of polar auxin transport by AtPIN1 in Arabidopsis vascular tissue. *Science* **282**: 2226–2230.

Gendre D, **Jonsson K**, **Boutte Y**, **Bhalerao RP. 2015**. Journey to the cell surface-the central role of the trans-Golgi network in plants. *Protoplasma* **252**: 385–398.

Hager A, **Debus G**, **Edel HG**, **Stransky H**, **Serrano R. 1991**. Auxin induces exocytosis and the rapid synthesis of a high turnover pool of plasma-membrane H^+-ATPase. *Planta* **185**: 527–537.

Harholt J, **Jensen JK**, **Sorensen SO**, **Orfila C**, **Pauly M**, **Scheller HV. 2006**. ARABINAN DEFICIENT 1 is a putative arabinosyltransferase involved in biosynthesis of pectic arabinan in Arabidopsis. *Plant Physiology* **140**: 49–58.

Havelkova L, **Nanda G**, **Martinek J**, ***et al.* 2015**. Arp2/3 complex subunit ARPC2 binds to microtubules. *Plant Science* **241**: 96–108.

Hepler PK, **Winship LJ. 2015**. The pollen tube clear zone: clues to the mechanism of polarized growth. *Journal of Integrative Plant Biology* **57**: 79–92.

Kandasamy MK, **McKinney EC**, **Meagher RB. 2009**. A single vegetative actin isovariant overexpressed under the control of multiple regulatory sequences is sufficient for normal Arabidopsis development. *Plant Cell* **21**: 701–718.

Ketelaar T. 2013. The actin cytoskeleton in root hairs: all is fine at the tip. *Current Opinion in Plant Biology* **16**: 749–756.

Kim SJ, **Brandizzi F. 2014**. The plant secretory pathway: an essential factory for building the plant cell wall. *Plant and Cell Physiology* **55**: 687–693.

Klahre U, **Chua NH. 1999**. The Arabidopsis ACTIN-RELATED PROTEIN 2 (AtARP2) promoter directs expression in xylem precursor cells and pollen. *Plant Molecular Biology* **41**: 65–73.

Kotchoni SO, **Zakharova T**, **Mallery EL**, **Le J**, **El-Assal SE**, **Szymanski DB. 2009**. The Association of the Arabidopsis actin-related protein2/3 complex with cell membranes is linked to its assembly status but not its activation. *Plant Physiology* **151**: 2095–2109.

Krupková E, **Immerzeel P**, **Pauly M**, ***et al.* 2007**. The TUMOROUS SHOOT DEVELOPMENT2 gene of Arabidopsis encoding a putative methyltransferase is required for cell adhesion and co-ordinated plant development. *Plant Journal* **50**: 735–750.

Lanza M, **Garcia-Ponce B**, **Castrillo G**, ***et al.* 2012**. Role of actin cytoskeleton in brassinosteroid signaling and in its integration with the auxin response in plants. *Developmental Cell* **22**: 1275–1285.

Le J, **El Assal SED**, **Basu D**, **Saad ME**, **Szymanski DB. 2003**. Requirements for Arabidopsis ATARP2 and ATARP3 during epidermal development. *Current Biology* **13**: 1341–1347.

Le J, **Mallery EL**, **Zhang CH**, **Brankle S**, **Szymanski DB. 2006**. Arabidopsis BRICK1/HSPC300 is an essential WAVE-complex subunit that selectively stabilizes the Arp2/3 activator SCAR2. *Current Biology* **16**: 895–901.

Ledbetter MC, **Porter KR. 1963**. A "microtubule" in plant cell fine structure. *The Journal of Cell Biology* **19**: 239–50.

Lewis DR, **Muday GK. 2009**. Measurement of auxin transport in *Arabidopsis thaliana*. *Nature Protocols* **4**: 437–451.

Li SD, **Blanchoin L**, **Yang ZB**, **Lord EM. 2003**. The putative Arabidopsis Arp2/3 complex controls leaf cell morphogenesis. *Plant Physiology* **132**: 2034–2044.

Li S, **Lei L**, **Somerville CR**, **Gu Y. 2012**. Cellulose synthase interactive protein 1 (CSI1) links microtubules and cellulose synthase complexes. *Proceedings of the National Academy of Sciences USA* **109**: 185–190.

Li X, **Li JH**, **Wang W**, ***et al.* 2014**. ARP2/3 complex-mediated actin dynamics is required for hydrogen peroxide-induced stomatal closure in Arabidopsis. *Plant Cell and Environment* **37**: 1548–1560.

Li YH, **Sorefan K**, **Hemmann G**, **Bevan MW. 2004**. Arabidopsis NAP and PIR regulate actin-based cell morphogenesis and multiple developmental processes. *Plant Physiology* **136**: 3616–3627.

Mathur J, **Spielhofer P**, **Kost B**, **Chua NH. 1999**. The actin cytoskeleton is required to elaborate and maintain spatial patterning during trichome cell morphogenesis in *Arabidopsis thaliana*. *Development* **126**: 5559–5568.

Mathur J, **Mathur N**, **Kernebeck B**, **Hulskamp M. 2003***a*. Mutations in actin-related proteins 2 and 3 affect cell shape development in Arabidopsis. *Plant Cell* **15**: 1632–1645.

Mathur J, **Mathur N**, **Kirik V**, **Kernebeck B**, **Srinivas BP**, **Hulskamp M. 2003***b*. Arabidopsis CROOKED encodes for the smallest subunit of the ARP2/3 complex and controls cell shape by region specific fine F-actin formation. *Development* **130**: 3137–3146.

Mouille G, **Ralet MC**, **Cavelier C**, ***et al.* 2007**. Homogalacturonan synthesis in *Arabidopsis thaliana* requires a Golgi-localized protein with a putative methyltransferase domain. *Plant Journal* **50**: 605–614.

Nakayama N, **Smith RS**, **Mandel T**, ***et al.* 2012**. Mechanical regulation of auxin-mediated growth. *Current Biology* **22**: 1468–1476.

Neumetzler L, **Humphrey T**, **Lumba S**, ***et al.* 2012**. The FRIABLE1 gene product affects cell adhesion in Arabidopsis. *Plos One* **7**: e42914.

Nick P. 2009. Probing the actin-auxin oscillator. *Plant Signal Behavior* **5**: 94–98.

Nolen BJ, **Pollard TD. 2007**. Insights into the influence of nucleotides on actin family proteins from seven structures of Arp2/3 complex. *Molecular Cell* **26**: 449–457.

Okada K, **Ueda J**, **Komaki MK**, **Bell CJ**, **Shimura Y. 1991**. Requirement of the auxin polar transport system in early stages of Arabidopsis floral bud formation. *The Plant Cell* **3**: 677–684.

Paque S, **Mouille G**, **Grandont L**, ***et al.* 2014**. AUXIN BINDING PROTEIN1 links cell wall remodeling, auxin signaling, and cell expansion in arabidopsis. *The Plant Cell* **26**: 280–95.

Paredez AR, **Somerville CR**, **Ehrhardt DW. 2006**. Visualization of cellulose synthase demonstrates functional association with microtubules. *Science* **312**: 1491–1495.

Parry G, **Delbarre A**, **Marchant A**, ***et al.* 2001**. Novel auxin transport inhibitors phenocopy the auxin influx carrier mutation aux1. *Plant Journal* **25**: 399–406.

Peremyslov VV, **Prokhnevsky AI**, **Dolja VV. 2010**. Class XI myosins are required for development, cell expansion, and F-actin organization in Arabidopsis. *Plant Cell* **22**: 1883–1897.

Peremyslov VV, **Cole RA**, **Fowler JE**, **Dolja VV. 2015**. Myosin-powered membrane compartment drives cytoplasmic streaming, cell expansion and plant development. *Plos One* **10**: e0139331.

Pitaksaringkarn W, **Matsuoka K**, **Asahina M**, ***et al.* 2014**. XTH20 and XTH19 regulated by ANAC071 under auxin flow are involved in cell proliferation in incised Arabidopsis inflorescence stems. *Plant Journal* **80**: 604–614.

Qiu JL, **Jilk R**, **Marks MD**, **Szymanski DB. 2002**. The Arabidopsis SPIKE1 gene is required for normal cell shape control and tissue development. *Plant Cell* **14**: 101–118.

Qiu L, **Lin JS**, **Xu J**, ***et al.* 2015**. SCARN a novel class of SCAR protein that is required for root-hair infection during legume nodulation. *PLoS Genetics* **11**: 1–27.

Ranocha P, **Denancé N**, **Vanholme R**, ***et al.* 2010**. Walls are thin 1 (WAT1), an Arabidopsis homolog of Medicago truncatula NODULIN21, is a tonoplast-localized protein required for secondary wall formation in fibers. *The Plant Journal* **63**: 469–483.

Ranocha P, **Dima O**, **Nagy R**, ***et al.* 2013**. Arabidopsis WAT1 is a vacuolar auxin transport facilitator required for auxin homoeostasis. *Nature Communications* **4**: 2625.

Ren H, **Dang X**, **Yang Y**, ***et al.* 2016**. SPIKE1 activates ROP GTPase to modulate petal growth and shape. *Plant physiology* **172**: 358–371.

Rounds CM, **Hepler PK**, **Winship LJ. 2014**. The apical actin fringe contributes to localized cell wall deposition and polarized growth in the lily pollen tube. *Plant Physiology* **166**: 139–151.

Saedler R, **Mathur N**, **Srinivas BP**, **Kernebeck B**, **Hulskamp M**, **Mathur J. 2004***a*. Actin control over microtubules suggested by DISTORTED2 encoding the Arabidopsis ARPC2 subunit homolog. *Plant and Cell Physiology* **45**: 813–822.

Saedler R, **Zimmermann I**, **Mutondo M**, **Hulskamp M. 2004***b*. The Arabidopsis KLUNKER gene controls cell shape changes and encodes the AtSRA1 homolog. *Plant Molecular Biology* **56**: 775–782.

Sampathkumar A, **Krupinski P**, **Wightman R**, ***et al.* 2014**. Subcellular and supracellular mechanical stress prescribes cytoskeleton behavior in Arabidopsis cotyledon pavement cells. *Elife* **3**: e01967.

Sampathkumar A, **Gutierrez R**, **McFarlane HE**, ***et al.* 2013**. Patterning and lifetime of plasma membrane-localized cellulose synthase is dependent on actin organization in Arabidopsis interphase cells. *Plant Physiology* **162**: 675–688.

Shao W, **Dong J. 2016**. Polarity in plant asymmetric cell division: division orientation and cell fate differentiation. *Developmental Biology* **419**: 121–131.

Scholl RL, **May ST**, **Ware DH. 2000**. Seed and molecular resources for Arabidopsis. *Plant Physiology* **124**: 1477–1480.

Schwab B, **Mathur J**, **Saedler RR**, ***et al.* 2003**. Regulation of cell expansion by the DISTORTED genes in *Arabidopsis thaliana*: actin controls the spatial organization of microtubules. *Molecular Genetics and Genomics* **269**: 350–360.

Soukup A. 2014. Selected simple methods of plant cell wall histochemistry and staining for light microscopy. In: Zarsky Viktor CF, eds. *Plant cell morphogenesis: methods and protocols. Totowa, NJ: Humana Press*, 25–40.

Swarup R, **Kargul J**, **Marchant A**, ***et al.* 2004**. Structure-function analysis of the presumptive Arabidopsis auxin permease AUX1. *Plant Cell* **16**: 3069–3083.

Szymanski DB, **Cosgrove DJ. 2009**. Dynamic coordination of cytoskeletal and cell wall systems during plant cell morphogenesis. *Current Biology* **19**: R800–R811.

Szymanski DB, **Marks MD**, **Wick SM. 1999**. Organized F-actin is essential for normal trichome morphogenesis in Arabidopsis. *Plant Cell* **11**: 2331–2347.

Takahashi K, **Hayashi K**, **Kinoshita T. 2012**. Auxin activates the plasma membrane H^+-ATPase by phosphorylation during hypocotyl elongation in Arabidopsis. *Plant Physiology* **159**: 632.

Ulmasov T, **Murfett J**, **Hagen G**, **Guilfoyle TJ. 1997**. Aux/IAA proteins repress expression of reporter genes containing natural and highly active synthetic auxin response elements. *Plant Cell* **9**: 1963–1971.

Updegraff DM. 1969. Semimicro determination of cellulose in biological materials. *Analytical Biochemistry* **32**: 420–424.

Van Gestel K, **Slegers H**, **Von Witsch M**, ***et al.* 2003**. Immunological evidence for the presence of plant homologues of the actin-related protein Arp3 in tobacco and maize: subcellular localization to actin-enriched pit fields and emerging root hairs. *Protoplasma* **222**: 45–52.

Vazquez LAB, **Sanchez R**, **Hernandez-Barrera A**, ***et al.* 2014**. Actin polymerization drives polar growth in Arabidopsis root hair cells. *Plant Signaling & Behavior* **9**: e29401.

Wang PW, **Richardson C**, **Hawes C**, **Hussey PJ. 2016**. Arabidopsis NAP1 regulates the formation of autophagosomes. *Current Biology* **26**: 2060–2069.

Xu T, **Dai N**, **Chen J**, ***et al.* 2014**. Cell surface ABP1-TMK auxin-sensing complex activates ROP GTPase signaling. *Science* **343**: 1025–1028.

Yanagisawa M, **Desyatova AS**, **Belteton SA**, **Mallery EL**, **Turner JA**, **Szymanski DB. 2015**. Patterning mechanisms of cytoskeletal and cell wall systems during leaf trichome morphogenesis. *Nature Plants* **1**: 1–8.

Zhang C, **Mallery EL**, **Schlueter J**, ***et al.* 2008**. Arabidopsis SCARs function interchangeably to meet actin-related protein 2/3 activation thresholds during morphogenesis. *Plant Cell* **20**: 995–1011.

Zhang C, **Mallery E**, **Reagan S**, **Boyko VP**, **Kotchoni SO**, **Szymanski DB. 2013***a*. The Endoplasmic reticulum is a reservoir for WAVE/SCAR regulatory complex signaling in the Arabidopsis leaf. *Plant Physiology* **162**: 689–706.

Zhang C, **Mallery EL**, **Szymanski D. 2013***b*. ARP2/3 localization in Arabidopsis leaf pavement cells: a diversity of intracellular pools and cytoskeletal interactions. *Frontiers in Plant Science* **4**: 238.

Zhang XG, **Dyachok J**, **Krishnakumar S**, **Smith LG**, **Oppenheimer DG. 2005**. IRREGULAR TRICHOME BRANCH1 in Arabidopsis encodes a plant homolog of the actin-related protein2/3 complex activator Scar/WAVE that regulates actin and microtubule organization. *Plant Cell* **17**: 2314–2326.

Zhu J, **Geisler M. 2015**. Keeping it all together: auxin-actin crosstalk in plant development. *Journal of Experimental Botany* **66**: 4983–4998.

Zou JJ, **Zheng ZY**, **Xue S**, **Li HH**, **Wang YR**, **Le J. 2016**. The role of Arabidopsis Actin-Related Protein 3 in amyloplast sedimentation and polar auxin transport in root gravitropism. *Journal of Experimental Botany* **67**: 5325–5337.